

Synthesis and Electronic Phosphorescence of Dicyanooctatetrayne (NCN) in Cryogenic Matrixes

Urszula Szczepaniak, Robert Kolos, Marcin Gronowski, Michèle Chevalier,
Jean-Claude Guillemin, Claudine Crépin

► **To cite this version:**

Urszula Szczepaniak, Robert Kolos, Marcin Gronowski, Michèle Chevalier, Jean-Claude Guillemin, et al.. Synthesis and Electronic Phosphorescence of Dicyanooctatetrayne (NCN) in Cryogenic Matrixes. *Journal of Physical Chemistry A*, American Chemical Society, 2018, 122 (25), pp.5580-5588. 10.1021/acs.jpca.8b02700 . hal-01834002

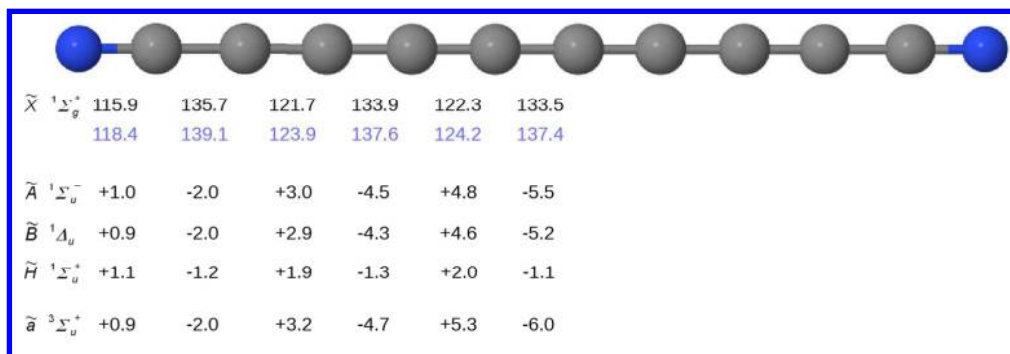
HAL Id: hal-01834002

<https://hal-univ-rennes1.archives-ouvertes.fr/hal-01834002>

Submitted on 13 Jul 2018

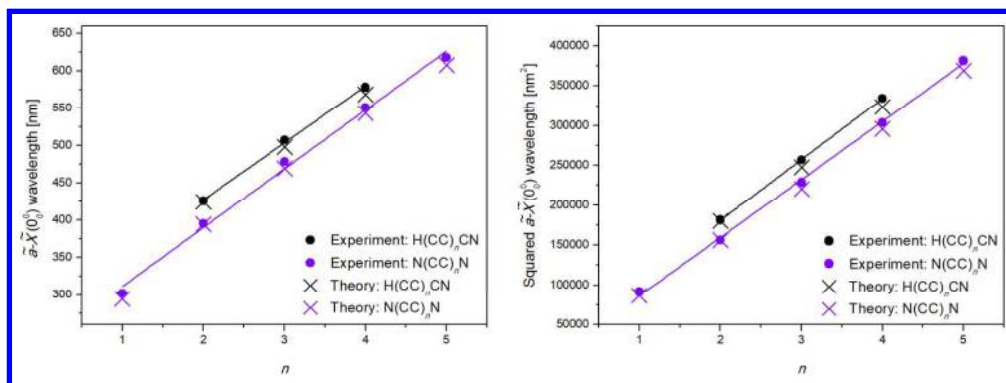
HAL is a multi-disciplinary open access archive for the deposit and dissemination of scientific research documents, whether they are published or not. The documents may come from teaching and research institutions in France or abroad, or from public or private research centers.

L'archive ouverte pluridisciplinaire **HAL**, est destinée au dépôt et à la diffusion de documents scientifiques de niveau recherche, publiés ou non, émanant des établissements d'enseignement et de recherche français ou étrangers, des laboratoires publics ou privés.



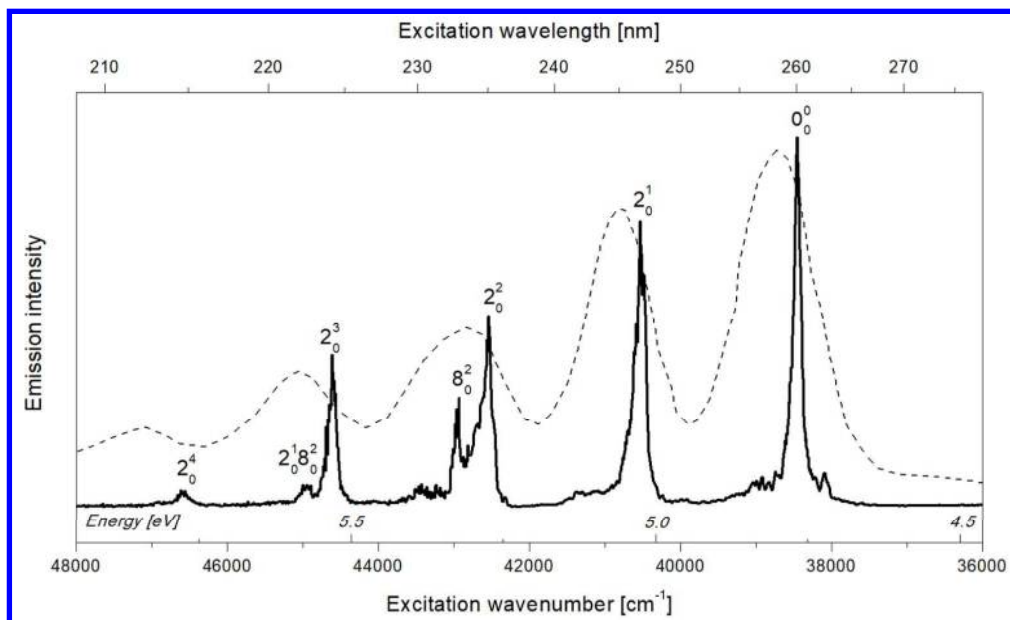
NC10N geometry in its ground and selected excited electronic states...

495x166mm (96 x 96 DPI)



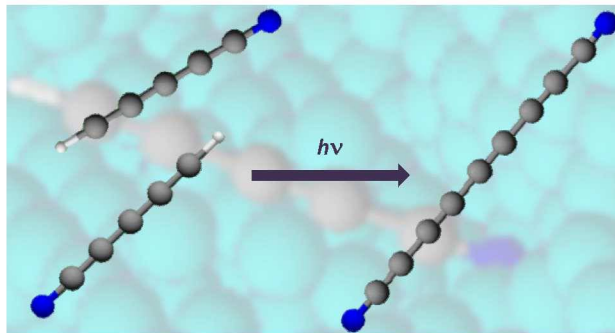
The dependence of phosphorescence wavelength...

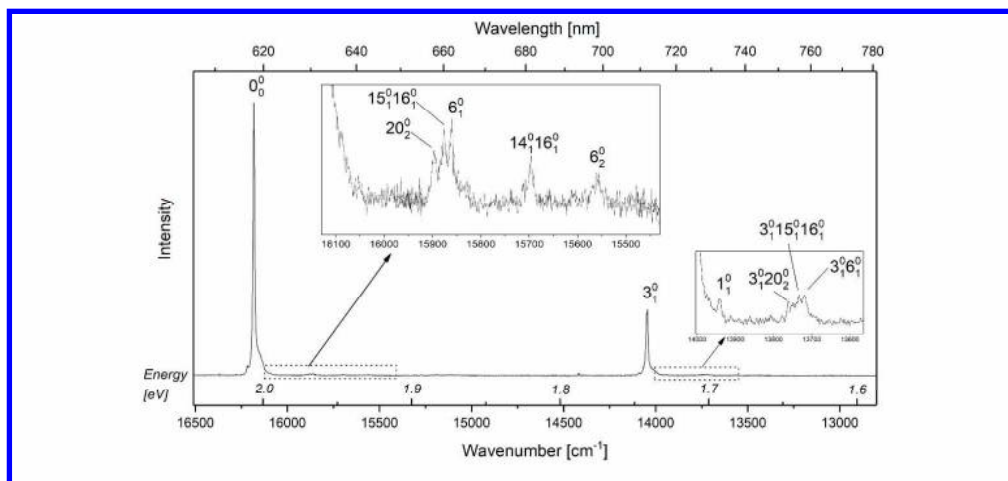
468x171mm (96 x 96 DPI)



Excitation spectrum of NC10N phosphorescence...

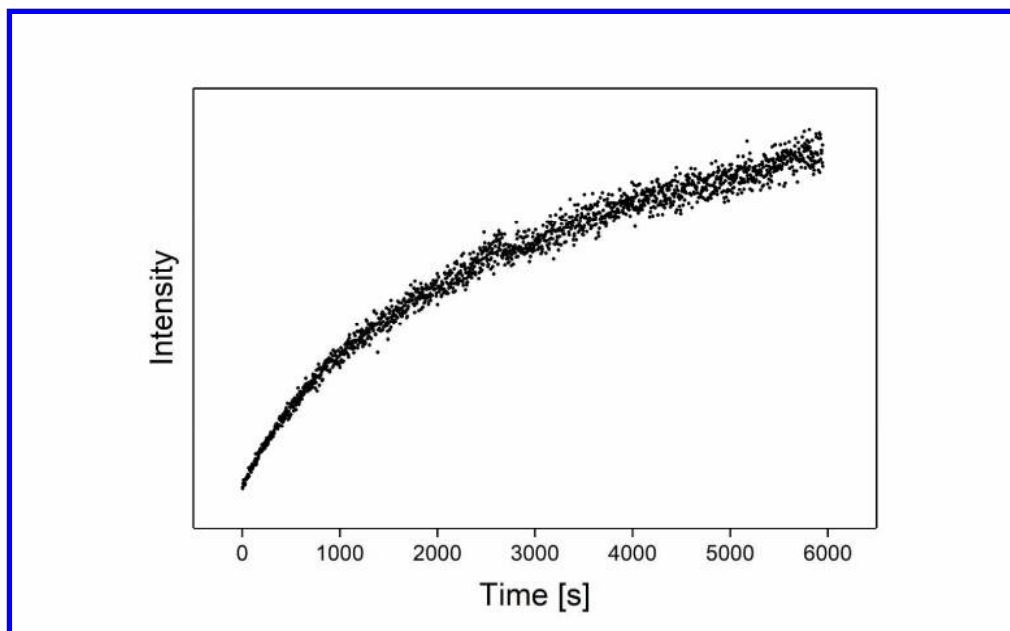
400x242mm (96 x 96 DPI)





Luminescence, assigned to NC10N phosphorescence, from a previously photolysed (193 nm) Kr/HC5N (1000/1) matrix, excited at 38 390 cm⁻¹ (4.76 eV, 260.5 nm).

431x201mm (300 x 300 DPI)



Time evolution of NC10N formation, as monitored by intensity of phosphorescence emitted from irradiated (193 nm) Kr-isolated HC5N. The abscissa represents the irradiation time.

330x203mm (300 x 300 DPI)

Synthesis and Electronic Phosphorescence of Dicyanooctatetrayne (NC₁₀N) in Cryogenic Matrices

Urszula Szczepaniak,^{a, b *} Robert Kołos,^b Marcin Gronowski,^b Michèle Chevalier,^a Jean-Claude Guillemin,^c and Claudine Crépin^a

^a Institut des Sciences Moléculaires d'Orsay (ISMO), UMR8214, CNRS, Univ. Paris-Sud, Université Paris-Saclay, F-91405 Orsay, FRANCE,

^b Institute of Physical Chemistry, Polish Academy of Sciences, Kasprzaka 44/52, 01-224 Warsaw, POLAND,

^c Univ Rennes, Ecole Nationale Supérieure de Chimie de Rennes, CNRS, ISCR – UMR6226, F-35000 Rennes, France

* urszula.szczepaniak@u-psud.fr, uszczepaniak@ichf.edu.pl; Present address: Laboratory of Physical Chemistry, ETH Zürich, Vladimir-Prelog Weg 2, CH-8093 Zürich, Switzerland.

ABSTRACT

Rod-like 1,8-dicyano-octa-1,3,5,7-tetrayne (NC₁₀N) molecule was synthesized by UV-assisted coupling of rare-gas matrix-isolated cyanobutadiyne (HC₅N) molecules. Detection of NC₁₀N molecule was possible due to its strong orange-red (origin at 618 nm) electronic luminescence. Excitation spectra of this emission ($\tilde{a}^3\Sigma_u^+ - \tilde{X}^1\Sigma_g^+$ phosphorescence) gave access to studying the fully allowed $\tilde{H}^1\Sigma_u^+ - \tilde{X}^1\Sigma_g^+$ UV system of NC₁₀N. The identification of observed spectral features was assisted with quantum chemical calculations. Certain regularities shaping the electronic spectroscopy of NC_{2n}N molecules have been discussed.

INTRODUCTION

Hydrogenless centrosymmetric dicyanopolyynes (NC_{2n}N) constitute a unique series of well-defined linear molecules of closed-shell electronic structure. They are kinetically more stable, at least as judged by the first elements of the series, than respective isoelectronic species of the related monocyano-polyynes (HC_{2n+1}N) or polyynes (HC_{2n}H) series.¹ For example, while working with dicyanoethyne (NC₄N)² we could observe that it is much less susceptible to decomposition (by polymerization) than cyanobutadiyne (HC₅N)³ or hexatriyne (HC₆H).⁴ Rod-like NC_{2n}N chains, with their highly conjugated bonding and the ensuing semiconductive properties, are interesting from purely theoretical/spectroscopic point of view, but potential applications, as nanowires,⁵ were also hypothesized. Moreover, dicyanopolyyne molecules are of astrochemical interest.⁶ However, while the presence of HC_{2n+1}N nitriles in interstellar gas clouds has been confirmed with microwave spectroscopy up to $n = 4$,⁷⁻¹⁶ little is known about centrosymmetric NC_{2n}N molecules in any extraterrestrial sources, apart from a tentative identification¹⁷ of dicyanoacetylene (NC₄N) in the atmosphere of the Saturn's moon Titan. Aerosols build-up from related, highly unsaturated carbon-

nitrogen polymers may contribute to the Titan's characteristic orange haze.¹⁹ Some information about NC_{2n}N molecules in space can be obtained by observation of their protonated forms.¹⁸

Certain molecular properties were theoretically predicted for NC_{2n}N molecules, including the geometry, vibrational modes, and electronic transition energies; some of these were derived up to $n = 8$.^{5,20-22} NC_2N , NC_4N , and (to a lesser extent) NC_6N are rather well experimentally characterized, being available in macroscopic quantities via preparative organic synthesis. In particular, these are known to emit strong phosphorescence under cryogenic isolation conditions.^{21,23,24} Experimental data reported for larger ($n > 3$) members of the series are limited to NMR spectroscopy (in CDCl_3 , $n \leq 9$),¹ IR spectra of solid substances in NaCl ($n \leq 9$),¹ electronic absorption spectra in liquid organic solvents^{1,25-27} ($n \leq 9$) and in the gas phase ($n = 8$),⁵ and low temperature electronic phosphorescence ($n = 4$).^{21,22,24} Very recently, traces of a long-lived luminescence attributable to NC_{10}N were observed by us in a study primarily devoted to HC_9N spectroscopy.²⁸ In each of these cases, electronic emission was characterized by at least one prominent vibronic progression with a spacing of $2000 - 2300 \text{ cm}^{-1}$, typical of CC or CN triple-bond stretching modes. Luminescence was also observed for C_4N_2^+ , C_6N_2^+ , and C_8N_2^+ in cryogenic Ne matrices.^{29,30}

Here we report on synthesizing NC_{10}N (1,8-dicyano-octa-1,3,5,7-tetrayne or deca-2,4,6,8-tetrayne-1,8-dinitrile) in noble gas (Ar and Kr) matrices, using the method of cryogenic photochemical coupling, already proved useful for C_6N_2 ,²¹ as well as for the monocyanopolyynes HC_5N ,^{21,31} HC_7N ,³² and HC_9N .²⁸ Since NC_6N appeared in photolysed matrices doped with HC_3N ,²¹ NC_{10}N formation from HC_5N was anticipated, even though HC_5N molecules are larger than HC_3N and their movement in a matrix is even more restricted. The spectroscopic identification of products has been supported using density functional theory calculations of electronic and vibrational energy levels.

EXPERIMENTAL METHODS

Experimental details regarding matrix preparation and spectroscopic characterization of the photochemical products are only briefly summarized here, as these were recently described in our reports on HC_9N ²⁸ and $\text{CH}_3\text{C}_7\text{N}$.³³

Precursor molecule, HC_5N , was prepared with the method developed by Trolez and Guillemin.³ It was purified by pumping while kept at $T < 200\text{K}$, directly before the experiment. Solid krypton has been shown to permit strong and spectrally well-resolved luminescence of embedded cyanopolyynes.^{21,22} Therefore, it was used here (4.0, Messer), along with, more commonly applied in matrix-isolation spectroscopy, argon (6.0, Messer).

HC_5N molecules were mixed with noble gases at a ratio of 1:1000 to 1:500. The mixture was subsequently trapped on a sapphire substrate window held at either 30 K (Kr) or at 22 K (Ar) inside a closed-cycle helium refrigerator equipped with external CaF_2 windows. The typical amount of deposited gas was 6-8 mmol. Composition of the samples was verified with FTIR spectroscopy. The photochemical transformations were induced with UV irradiation of cryogenic matrices (30 K for Kr; 22 K for Ar) by means of an ArF excimer laser (193 nm, 10 Hz, $< 5\text{mJ}/\text{cm}^2$ per pulse). Spectra

1
2 80 were recorded for a sample kept at 7 K. Of note, the formation of NC₁₀N was also observed in
3 81 experiments aimed at HC₉N and CH₃C₇N, involving HC₅N co-deposited with, respectively,
4 82 diacetylene (see Ref. ²⁸) and methylacetylene (see Ref. ³³). Certain thus far unpublished results
5 83 coming from these studies are included in the present report.

6
7
8 84 The identification of photolysis products relied on selectively excited electronic luminescence, by
9 85 means of an optical parametric oscillator (OPO). Dispersed phosphorescence was searched for in the
10 86 380 – 800 nm range with a resolution of approx. 0.04 nm. The observed emission was also
11 87 registered as a function of the excitation wavelength (192 – 280 nm), yielding phosphorescence
12 88 excitation spectra. Time synchronization between laser pulses (193 nm excimer laser for photolysis
13 89 and a tunable OPO for spectroscopy), as well as the acquisition of phosphorescence signals (with a
14 90 CCD camera) were provided by a home-made triggering device.

15
16
17
18 91

19 92 COMPUTATIONAL DETAILS

20
21
22 93 Although certain theoretical studies devoted to NC₁₀N have already been reported,²⁰ these did not
23 94 comprise excited electronic states. Here, experiments implicated electronic excitation, respective
24 95 quantum chemical calculations were therefore performed; for consistency, predictions concerning
25 96 the ground electronic state have also been included.

26
27
28 97 Quantum chemical computations were carried out mainly at the density functional theory (DFT)³⁴
29 98 level, with the GAUSSIAN 09 (Rev. B. 01)³⁵ program package. Time-dependent methodologies^{36–38}
30 99 and the B3PW91 functional of Perdew and Wang^{39–42} were applied for singlet excited electronic
31 100 states. Energetic separations between the ground and the lowest triplet states were derived
32 101 employing the CAM-B3LYP⁴³ functional. Computations made use of the aug-cc-pVTZ^{44,45} basis set.
33 102 This approach supplied molecular geometries, harmonic vibrational wavenumbers, and energies of
34 103 transitions from the ground to excited electronic states. Additionally, IR absorption intensity and
35 104 Raman activity values were predicted for the ground electronic state (B3PW91/aug-cc-pVTZ). To
36 105 account for anharmonicity and inherent deficiencies of the involved theoretical approach, vibrational
37 106 wavenumbers were scaled with the factor of 0.96.^{46,47} Linearity of the carbon-nitrogen backbone in
38 107 excited singlet electronic states was verified by performing CIS/aug-cc-pVDZ^{44,45,48} optimizations
39 108 (starting from a bent structure) and by looking, at both CIS and DFT levels, for the degeneracy of
40 109 bending modes. Optimized structures were also checked for the absence of imaginary vibrational
41 110 frequencies. Vertical excitation energies, together with the corresponding oscillator strengths, were
42 111 additionally derived at the *ab-initio* level CC2^{49–52} (cc-pVTZ basis set), using the Dalton2016^{53,54}
43 112 software. Chemcraft⁵⁵ program was employed in the preparation of input data and for the
44 113 visualization of results. However, the CC2 approach applied here can not be regarded as inherently
45 114 more accurate than DFT, since our CC2 calculations were performed solely within the vertical
46 115 approximation.

47
48
49
50
51
52
53 116

54 117 RESULTS AND DISCUSSION

118 A. Theoretical predictions

119 Theoretical results concerning the electronic states of NC₁₀N are collected in Table 1 and Figure 1.
 120 The first fully allowed electronic excitation of a ground-state molecule is predicted at 4.65 eV (267
 121 nm). We have checked that the energy of the next allowed transition is around 6.2 eV (vertical
 122 approximation), and no transition with oscillator strength similar to that characterizing $\tilde{H} - \tilde{X}$ is
 123 predicted up to around 7 eV. Formerly reported UV-Vis absorption of NC₁₀N in acetonitrile¹ and in
 124 *n*-octane solution²⁵ is energetically close to the currently predicted $\tilde{H} - \tilde{X}$ excitation. Electronic
 125 structures characterizing states \tilde{A} , \tilde{B} , \tilde{a} , and \tilde{H} originate mainly in the HOMO-LUMO excitation. \tilde{H}
 126 state features the smallest deviation from the ground state geometry (see Figure 1), just as reported
 127 for the analogous (\tilde{E}) state of HC₉N.²⁸ Transitions to the three lowest excited states (\tilde{A} , \tilde{B} , and \tilde{a})
 128 result in mutually similar changes of geometry (in analogy to what was observed for several alike
 129 carbon-nitrogen chains^{28,33,56}).

130 **Table 1. Theoretical Predictions^a of Energy (in eV), Wavelength (in nm), and Oscillator Strength (*f*) for**
 131 **Electronic Transitions of NC₁₀N Departing from the $\tilde{X}^1\Sigma_g^+$ State^b.**

State	Dominant orbital excitation	CC2/cc-pVTZ		DFT		
		Vertical transition energy (wavelength)	<i>f</i>	Vertical transition energy (wavelength)	<i>f</i> ^c	0-0 transition energy (wavelength)
$\tilde{A}^1\Sigma_u^-$	$3\pi_g \rightarrow 1\pi_u^*$	3.27 (379)	0	2.62 (473)	0	2.18 (569)
$\tilde{B}^1\Delta_u$	$3\pi_g \rightarrow 1\pi_u^*$	3.39 (366)	0	2.71 (458)	0	2.30 (539)
$\tilde{C}^1\Sigma_g^-$	$3\pi_u \rightarrow 1\pi_u^*$	4.64 (267)	0	4.01 (309)	0	3.74 (332)
$\tilde{D}^1\Delta_g$	$3\pi_u \rightarrow 1\pi_u^*$	4.84 (256)	0	4.16 (298)	0	3.90 (318)
$\tilde{E}^1\Sigma_g^-$	$3\pi_g \rightarrow 1\pi_g^*$	5.92 (209)	0	4.81 (258)	0	4.53 (274)
$\tilde{F}^1\Delta_g$	$3\pi_g \rightarrow 1\pi_g^*$	6.01 (206)	0	4.82 (257)	0	4.54 (273)
$\tilde{G}^1\Sigma_g^+$	$3\pi_u \rightarrow 1\pi_u^*$ $3\pi_g \rightarrow 1\pi_g^*$	5.32 (233)	0	4.84 (256)	0	4.56 (272)
$\tilde{H}^1\Sigma_u^+$	$3\pi_g \rightarrow 1\pi_u^*$	5.30 (234)	6.1	4.80 (258)	5.2	4.65 (267)
$\tilde{a}^3\Sigma_u^+$	$3\pi_g \rightarrow 1\pi_u^*$	2.59 (479)				2.04 (608)

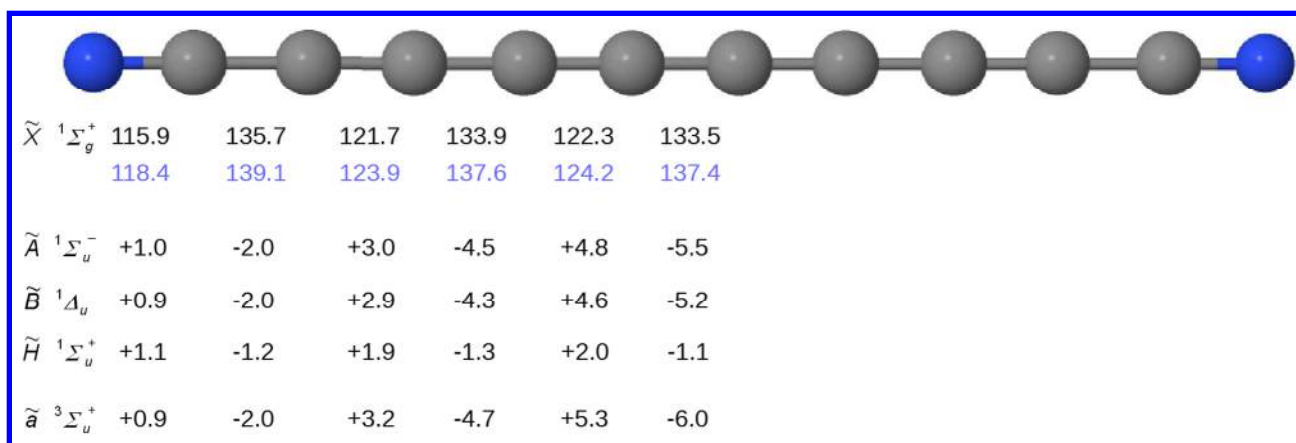
132 ^a Obtained with DFT (B3PW91/aug-cc-pVTZ for excited singlet states, CAM-B3LYP/aug-cc-pVTZ for $\tilde{a}^3\Sigma_u^+$) and *ab*
 133 *initio* (CC2/cc-pVTZ) methods.

134 ^b Ground state electronic configuration is [core] $(1\sigma_u)^2 (1\sigma_g)^2 (2\sigma_g)^2 (2\sigma_u)^2 (3\sigma_g)^2 (3\sigma_u)^2 (4\sigma_g)^2 (4\sigma_u)^2 (5\sigma_g)^2 (5\sigma_u)^2 (6\sigma_g)^2$
 135 $(1\pi_u)^4 (1\pi_g)^4 (2\pi_u)^4 (6\sigma_u)^2 (7\sigma_g)^2 (2\pi_g)^4 (3\pi_u)^4 (3\pi_g)^4 (1\pi_u^*)^0 (1\pi_g^*)^0 (1\sigma_g^*)^0$.

136 ^c 0 indicates $f < 5 \cdot 10^{-5}$.

137

138



139

140 **Figure 1.** NC₁₀N geometry in its ground and selected excited electronic states as derived at the B3PW91/aug-cc-
 141 pVTZ level of theory. Interatomic distances in pm. Values listed for the excited states are relative, calculated with
 142 respect to \tilde{X} . Also given (blue) are the RCCSD(T)/aug-cc-pVTZ predictions for the ground state.²⁰ Geometry
 143 predicted for other electronic states listed in Table 1 can be found in Figure S1 of the Supporting Information.

144

145 Table 2 lists DFT-derived wavenumbers, IR intensities and Raman activities for the vibrational
 146 modes of the ground electronic state, together with respective \tilde{H} -state values (see Table S1 of the
 147 Supporting Information for the data concerning other excited electronic states). The visualization of
 148 vibrational modes is presented in Table S2 of the Supporting Information.

149 IR absorption measurements for NC₁₀N dispersed in a solid NaCl film¹ pointed to the spectral
 150 features at 2237 cm⁻¹ (the strongest one, assigned to CN stretching), 2186, and 2120 cm⁻¹; the first
 151 two match well our present prediction of the strongest IR fundamentals (ν_7 and ν_8).

152 **Table 2.** Wavenumbers^a of Vibrational Modes ($\tilde{\nu}$, in cm⁻¹; scaled by 0.96) for $\tilde{X} \ ^1\Sigma_g^+$ and $\tilde{H} \ ^1\Sigma_u^+$ Electronic States
 153 of NC₁₀N. ^b Absolute IR Absorption Intensity (in km/mol) and Raman Scattering Activity (in Å⁴/amu) Values^a for
 154 $\tilde{X} \ ^1\Sigma_g^+$ State.

Mode	Symmetry	\tilde{X}			\tilde{H}
		$\tilde{\nu}$	IR intensity	Raman activity	$\tilde{\nu}$
σ symmetry					
ν_1	σ_g	2254	0	7200	2194
ν_2	σ_g	2140	0	150	2067
ν_3	σ_g	2115	0	74000	2017
ν_4	σ_g	1414	0	25	1431
ν_5	σ_g	908	0	52	911
ν_6	σ_g	314	0	4.6	315
ν_7	σ_u	2241	280	0	2174
ν_8	σ_u	2199	20	0	2096
ν_9	σ_u	2061	0.015	0	1941
ν_{10}	σ_u	1180	0.016	0	1190
ν_{11}	σ_u	617	1.1	0	621
π symmetry					
ν_{12}	π_g	554	0	146	509
ν_{13}	π_g	512	0	1.8	462
ν_{14}	π_g	437	0	0.55	392
ν_{15}	π_g	222	0	0.61	210

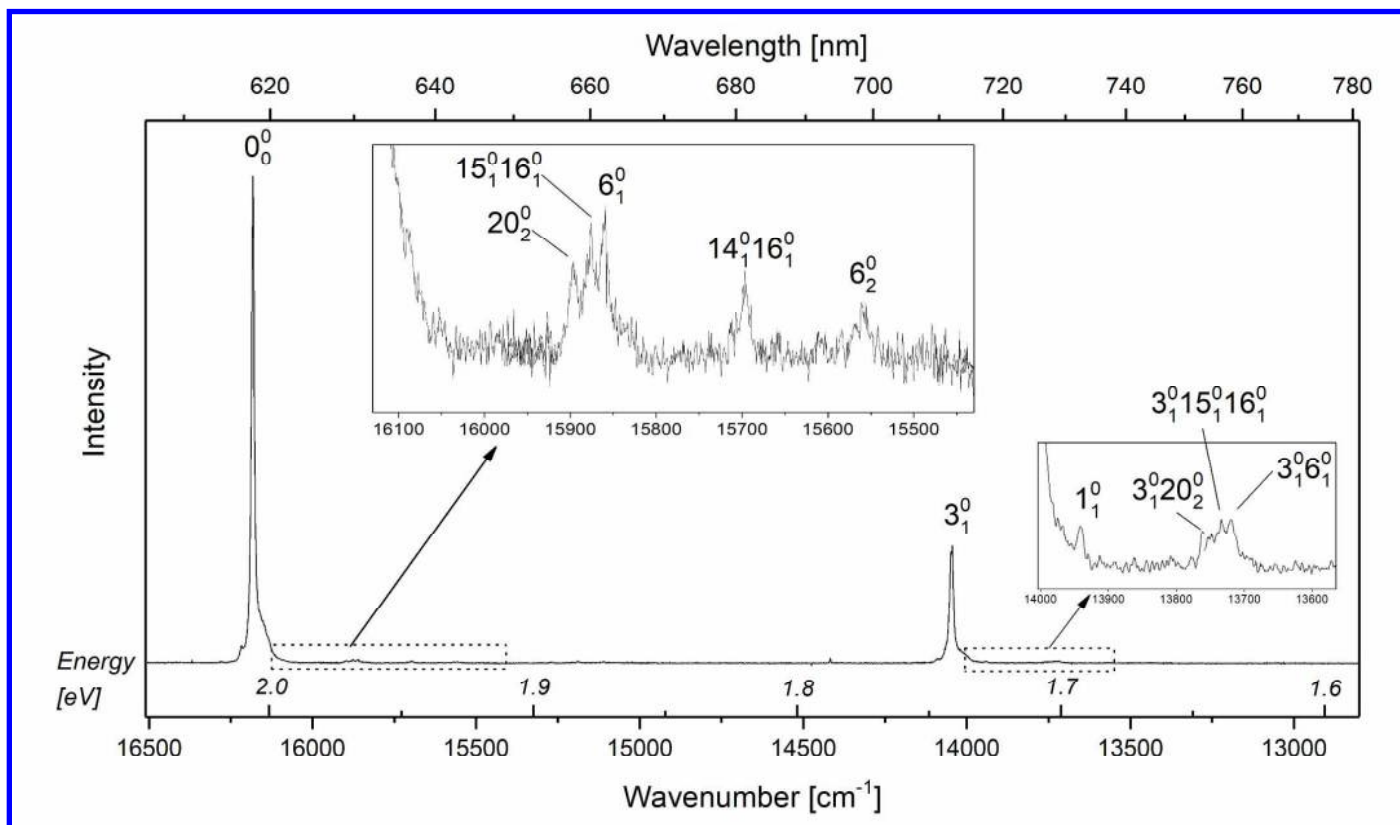
ν_{16}	π_g	75	0	0.091	75
ν_{17}	π_u	561	3.4	0	515
ν_{18}	π_u	492	11	0	455
ν_{19}	π_u	308	7.0	0	288
ν_{20}	π_u	142	11	0	139
ν_{21}	π_u	28	5.2	0	30

^a Derived with harmonic approximation at the B3PW91/aug-cc-pVTZ level of theory.

^b See Table S2 of the Supporting Information for the visualization of vibrational modes.

B. Electronic luminescence

A strong vibronic progression beginning around 615 nm, excited close to 260 nm, appeared in luminescence of HC₅N-doped rare gas matrices previously subjected to ArF-laser irradiations (Figure 2). The new emission can be recognized as phosphorescence of NC₁₀N, based on (i) location of the strongest band (16 183 cm⁻¹ or 2.01 eV in Kr), a straightforward candidate for the vibrationless origin, matching the theoretical prediction for the $\tilde{a}^3\Sigma_u^+ - \tilde{X}^1\Sigma_g^+$ system (2.04 eV, gas phase); (ii) vibronic spacing (~2140 cm⁻¹; characteristic of a triple-bond stretching); (iii) long luminescence decay time (4.4 ms in Kr); (iv) the nature of precursor species (conceivably capable of doubling its heavy-atom backbone length, just as HC₃N molecules were shown to yield NC₆N).²¹ Furthermore, the indicated vibrationless origin (618 nm in Kr or 612.6 nm in Ar) fits well to the general trend already observed for shorter NC_{2*n*}N molecules (see later in the text).



169

170

171 **Figure 2. Luminescence, assigned to NC₁₀N phosphorescence, from a previously photolysed (193 nm) Kr/HC₅N**
 172 **(1000/1) matrix, excited at 38 390 cm⁻¹ (4.76 eV, 260.5 nm).**

173 The observed main vibronic spacing (see Figure 2) may originate in one of the two *gerade*
 174 stretchings, either ν_3 or ν_2 , with DFT-predicted wavenumbers of 2115 cm^{-1} and 2140 cm^{-1} ,
 175 respectively. Although this last value better matches the observed separation of progression
 176 elements, the former is preferred, based on its particular molecular distortion pattern: alternate
 177 shrinking-expansion of interatomic distances along the chain (see Table S2), qualitatively similar to
 178 the geometry change experienced by NC_{10}N upon the transition from \tilde{X} to \tilde{a} (Figure 1). Moreover,
 179 the ν_3 stretching is distinct by its highest Raman scattering activity (see Table 2), and such modes
 180 were already shown to shape the main vibronic progressions of phosphorescence emitted by shorter
 181 NC_{2n}N molecules.^{2,21–23,57} Table 3 lists all vibronic bands presently identified in the $\tilde{a} \ ^3\Sigma_u^+ - \tilde{X} \ ^1\Sigma_g^+$
 182 system of NC_{10}N . The appearance of only one strong progression governed by a single mode (C \equiv C
 183 stretching), with very few other vibrations contributing to the recognized weak bands, is consistent
 184 with the linearity of the lowest triplet state, predicted by DFT calculations. One can notice that in the
 185 phosphorescence of NC_{2n}N molecules, relative intensity of bands that do not involve the specific
 186 C \equiv C stretching (analogous to ν_3 here) diminishes with n growing from 2 to 5.^{2,57}

187 Weak phosphorescence bands appearing in Kr matrices, blue-shifted from the main spectral
 188 features, can be clearly assigned, to a minor matrix site (origin at 16220 cm^{-1}), based on
 189 phosphorescence excitation spectra (see below). In Ar-matrix spectra (the Kr-Ar matrix shift is quite
 190 large, see Table 3), only the strongest bands have been identified.

191 **Table 3. Vibronic Bands in NC_{10}N Phosphorescence. Relative Values Give the Distance from the Vibrationless**
 192 **Origin.**

Wavenumber [cm^{-1}]				Assignment
Kr		Ar		
Absolute	Relative	Absolute	Relative	
16183	0	16324	0	0_0^0
15897	286			20_2^0
15880	303			$15_1^0 16_1^0$
15861	322			6_1^0
15699	484			$14_1^0 16_1^0$
15617 ^a	566			$6_1^0 20_2^0$
15585 ^a	598			$6_1^0 15_1^0 16_1^0$
15562 ^a	621			6_2^0
14046	2137	14186	2138	3_1^0
13941	2242			1_1^0
13760	2423			$3_1^0 20_2^0$
13740	2443			$3_1^0 15_1^0 16_1^0$
13720	2463			$3_1^0 6_1^0$

193 ^a Weak band, observed with wide-open monochromator slits.

194

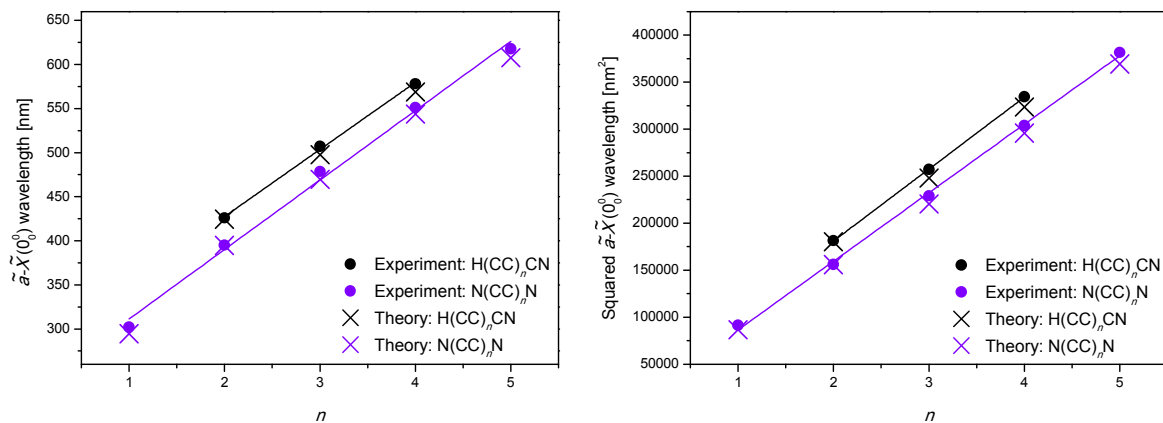
1
2 195 Table 4 collects the results of phosphorescence lifetime measurements for solid Kr-isolated mono-
3 196 and dicyanopolyynes. Within each of these families, emission lifetime markedly decreases with the
4 197 increase of polyynes length, a trend that may be explained considering the associated enhancement of
5 198 two factors promoting non-radiative $T_1 \rightarrow S_0$ relaxation channels: reduction of the singlet-triplet gap
6 199 and the increasing number of vibrational degrees of freedom (leading to high density of states).
7 200 Monocyanopolyynes of Table 4 are characterized by faster phosphorescence decays than the
8 201 respective (*i.e.* isoelectronic) dicyanopolyynes, which may again be due to the higher number of
9 202 vibrational modes of the former. Moreover, one may point to a possible special role of large CH
10 203 stretching quanta in coupling T_1 with the ground electronic state.

14 204 **Table 4. Phosphorescence Decay Time (in ms) for Mono- and Dicyanopolyynes Isolated in Solid Kr.**

HC _n N	τ	NC _n N	τ
HC ₅ N ^a	40	NC ₄ N ^b	52
HC ₇ N ^c	8	NC ₆ N ^d	35
HC ₉ N ^e	3.9	NC ₈ N ^d	13
		NC ₁₀ N ^f	4.4

23 205 ^a From Ref. ⁵⁸. ^b From Ref. ². ^c From Ref. ³³. ^d From Ref. ⁵⁷. ^e From Ref. ²⁸. ^f This work.

24 206
25 207 A systematic change of electronic transition energy with the molecular size is expected to occur in
26 208 homologous series (in particular those of unsaturated carbon-chain molecules) for vibrationless
27 209 transitions sharing a common electronic provenance.⁵⁹ Such regularities can be simplistically
28 210 described either by a particle-in-a-box model (where a ‘particle’, *i.e.* an electron, is delocalized in a
29 211 ‘box’ formed by a system of conjugated bonds)⁶⁰ or by a harmonic oscillator model (with electrons
30 212 oscillating within π orbitals).⁶¹ It should then be manifested, respectively, by the linear correlation of
31 213 chain size with either λ_{origin} or $\lambda_{\text{origin}}^2$. Forney et al.⁶² reported on linear λ_{origin} vs. n relations for
32 214 the first allowed electronic absorption systems in several series of highly unsaturated carbon-
33 215 backbone molecules: HC_{2n+1}N⁺, NC_{2n}N⁺, HC_{2n}N⁺, and NC_{2n+1}N⁺. The same properties have been
34 216 found for C_{2n}H⁻, C_{2n+1}H⁻, HC_{2n}H⁻, HC_{2n+1}H⁺, HC_{2n+1}H, C_{2n+1}, and C_{2n+1}⁻ families.⁶³ This can be
35 217 rationalized in terms of a high delocalization of electrons involved in the considered transitions. On
36 218 the other hand, certain curvature of λ_{origin} vs. n plots, evident for $n > 4$ in the neutral polyynes
37 219 (HC_{2n}H) series, was associated by Pino et al.⁶³ with more pronounced localization of π orbitals. In
38 220 such cases, as demonstrated by Hausser et al.⁶⁴ for diphenylpolyenes, a $\lambda_{\text{origin}}^2$ vs. n relation (Lewis-
39 221 Calvin plot) is expected to offer good linearity. Figure 3 presents the $\tilde{\nu} - \tilde{X}$ vibrationless origin
40 222 wavelength data for NC_{2n}N, and also for the recently analyzed HC_{2n+1}N series. These are neutral,
41 223 closed-shell structures just as unsubstituted polyynes. Indeed, slightly better linear fits are obtained
42 224 when $\lambda_{\text{origin}}^2(n)$ rather than $\lambda_{\text{origin}}(n)$ relation is applied. This can be best seen for the largest (5-
43 225 element) sequence of values collected here, *i.e.* dicyanopolyynes.



226

227 **Figure 3. The dependence of phosphorescence wavelength λ_{origin} (left panel) and $\lambda_{\text{origin}}^2$ (right panel) on**
 228 **molecular size, for the series of cyanopolyynic molecules photochemically formed in solid Kr. Experimental**
 229 **values for NC_2N , NC_4N , NC_6N , and NC_8N come from Refs. 2,21–23. Theoretical values as derived at CAM-**
 230 **B3LYP/aug-cc-pVTZ level of theory. Experimental values were fitted with linear functions. The R2 values of fits**
 231 **for dicyanopolyynes are 0.999 and 0.995 for the quadratic and linear functions, respectively. Respective values**
 232 **for monocyanopolyynes are: 0.99997 and 0.99856.**

233

234 Lines defined by NC_{2n}N and HC_{2n+1}N data (Figure 3) appear to be parallel to each other (with a
 235 slope of approx. 75 000 nm²/triple bond). This can be interpreted as the inclusion of an extra $-\text{C}\equiv\text{C}-$
 236 unit having the same effect in both series. It makes yet another similarity between the
 237 phosphorescence properties of respective di- and monocyano species. In case of the first fully
 238 allowed ($^1\Sigma_u^+ - ^1\Sigma_g^+$) system observed for NC_{2n}N ($n = 3$ to 8) solutions in acetonitrile (Ref. ¹), the
 239 slope of a Lewis-Calvin plot is much lower (~ 12 000 nm²/triple bond) than for the presently
 240 discussed phosphorescence, reflecting differences in electronic structure of the lowest triplet ($^3\Sigma_u^+$)
 241 and the lowest singlet ($^1\Sigma_u^+$) state (evidenced also by their dissimilar geometries; see Figure 1).

242

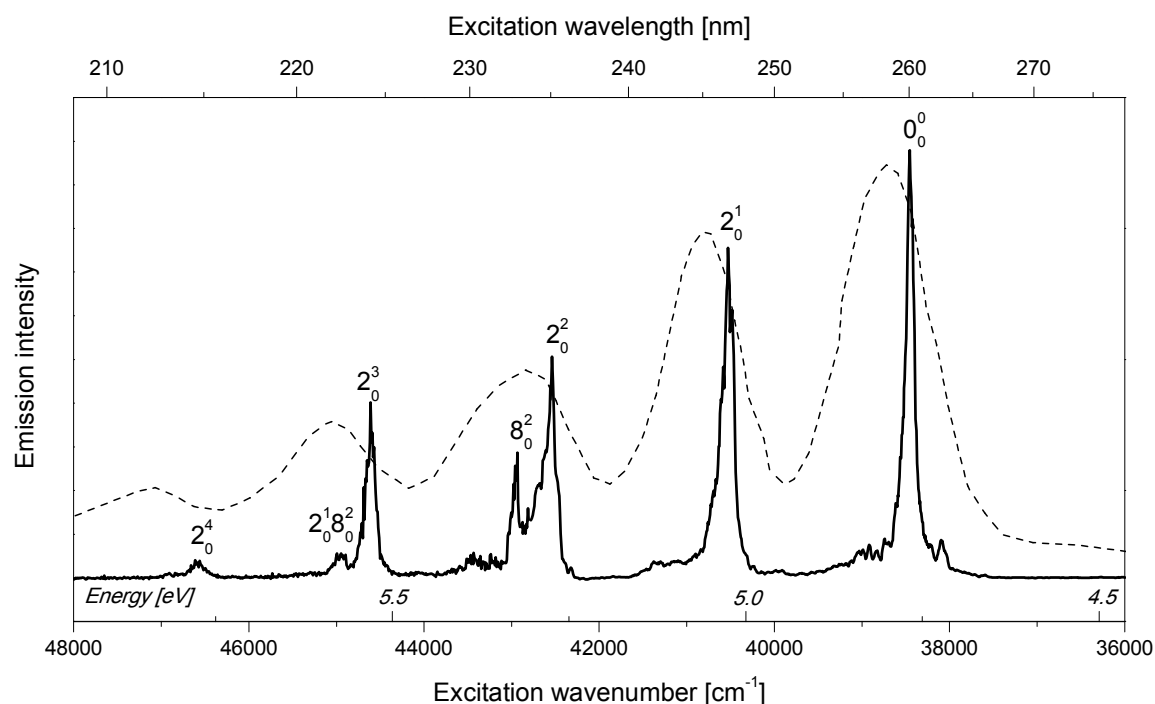
243 C. Singlet excited electronic states

244 The phosphorescence excitation spectrum of Kr matrix-isolated NC_{10}N is shown in Figure 4. The
 245 first intense band falls around 38 500 cm⁻¹ (4.77 eV, 260 nm), in good agreement with the predicted
 246 vibrationless onset of the fully allowed $\tilde{H} \ ^1\Sigma_u^+ - \tilde{X} \ ^1\Sigma_g^+$ system (4.65 eV). When identifying other
 247 vibronic bands, one should only consider the involvement of *g*-symmetry vibrations, *i.e.* those
 248 preserving the general $g \leftrightarrow u$ selection rule. The proposed assignments are presented in Table 5. We
 249 identify the \tilde{H} -state mode responsible for the main progression as ν_2 , considering that it distorts the
 250 molecule in the same way (all in-phase C \equiv C stretches; see Table S2 of the Supporting Information)
 251 as does the ν_3 mode of state \tilde{X} , recognized as the one shaping the vibronic structure of
 252 phosphorescence. Also, the calculated wavenumber of \tilde{H} -state ν_2 better matches the obtained
 253 spectral data than that of ν_3 . A weak distinct band observed to the red of the identified $\tilde{H} - \tilde{X}$ origin
 254 may be tentatively interpreted as due to a lower-lying electronic state, the excitation of which could
 255 gain probability *via* Herzberg–Teller vibronic coupling (analogous effects were already evidenced in

1
2 256 HC_{2n+1}N (*n* = 3, 4) excitation spectra in the region of the first allowed electronic bands).^{28,33} Weak
3 257 features detected to the blue of the main vibronic bands supposedly come from the coupling with
4 258 phonons and/or from the combination with low frequency bending modes; no reliable assignments
5 259 can be proposed.

6
7
8 260 Comparing Ar and Kr matrices, one can notice large differences (up to ~1000 cm⁻¹) in the position
9 261 of detected spectral features. Moreover, spectral splittings, observed in solid Kr, coming from
10 262 dissimilar surroundings of embedded molecules (matrix sites) vary between 20 and 180 cm⁻¹ (see
11 263 Table 5). This evidence points to substantial influence of the microenvironment on electronic
12 264 transitions of this highly polarizable²⁰ molecule. The role of environment was also demonstrated by
13 265 slightly differing band wavenumbers, from one sample to another. Due to all these effects and to the
14 266 high photon energy in the discussed spectral range, the error of measured wavenumber distances
15 267 could reach 30 cm⁻¹. Nevertheless, systematic irregularities observed in vibronic spacing reflect the
16 268 contributions from anharmonic interactions. As expected, Kr-to-Ar matrix shifts are larger for
17 269 $\tilde{H} - \tilde{X}$ than for $\tilde{a} - \tilde{X}$ transitions. The present Kr-matrix spectrum is compared in Figure 4 with the
18 270 UV absorption of NC₁₀N in liquid acetonitrile¹ (maxima at 259, 246, 235 and 223 nm). Neglecting
19 271 the widths of spectral features, and hence the number of resolved details, the two spectra resemble
20 272 one another. Moreover, just as for cryogenic matrix sample, vibronic spacings observed in liquid
21 273 acetonitrile are not regular. Another NC₁₀N absorption spectrum was reported²⁵ for a liquid *n*-octane
22 274 solution, with strong absorption bands at 283, 268, 253, 243, and 232 nm. However, an *n*-octane-to-
23 275 acetonitrile shift of approx. -3300 cm⁻¹ (283 nm²⁵ vs. 259 nm¹) is unrealistic, and the attribution
24 276 given in Ref. ²⁵ seems to be erroneous. Additionally, a ¹Σ_u⁺ - ¹Σ_g⁺ origin in the vicinity of 240 nm
25 277 can be deduced for gas-phase NC₁₀N from the interpolation of experimental data reported in Ref. ⁵,
26 278 indicating a gas-to-Kr matrix shift of ca. -3200 cm⁻¹. This large redshift is smaller than that due to
27 279 the matrix (>4000 cm⁻¹) observed for the origin of allowed NC₆N absorption (205 nm in Kr⁵⁷, 188
28 280 nm in gas phase⁶⁵).

29
30
31
32
33
34
35
36 281
37
38
39
40
41
42
43
44
45
46
47
48
49
50
51
52
53
54
55
56
57
58
59
60



282

283 **Figure 4.** Excitation spectrum of luminescence assigned to NC₁₀N phosphorescence detected at 16 183 cm⁻¹ (2.01
 284 eV), as measured for a photolyzed (193 nm) Kr/HC₅N (1000/1) matrix. UV absorption spectrum of NC₁₀N
 285 dissolved in liquid acetonitrile (dashed trace; digitized data from Ref. ¹) is given for comparison. Variations of the
 286 excitation laser fluence could distort the measured phosphorescence intensity pattern.

287

288 **Table 5.** Vibronic Bands in NC₁₀N Phosphorescence Excitation Spectrum, due to Dipole-Allowed $\tilde{H}^1\Sigma_u^+ - \tilde{X}^1\Sigma_g^+$
 289 Transitions. Relative Wavenumber Values Give Distances from the Preceding Progression Elements.

Wavenumber [cm ⁻¹]						Assignment
Kr matrix, main site		Kr matrix, minor site		Ar matrix		
Absolute	Relative	Absolute	Relative	Absolute	Relative	
38 470	0	38 610	0	39430	0	0 ₀ ⁰
40 540	2070	40 700	2090	41440	2010	2 ₀ ¹
42 550	2010	42 730	2030	43510	2070	2 ₀ ²
42 950	400	42 970	240			8 ₀ ²
44 600	2050	44 700	1970	45480	1970	2 ₀ ³
44 940	340	45 010	310			2 ₀ ¹ 8 ₀ ²
46 580	1980	46 680	1980			2 ₀ ⁴
46 910	330					2 ₀ ² 8 ₀ ²

290

291 D. Formation

292 Based on previous similar considerations^{28,33}, one can propose the following NC₁₀N formation
 293 scheme:



296 Radical recombination

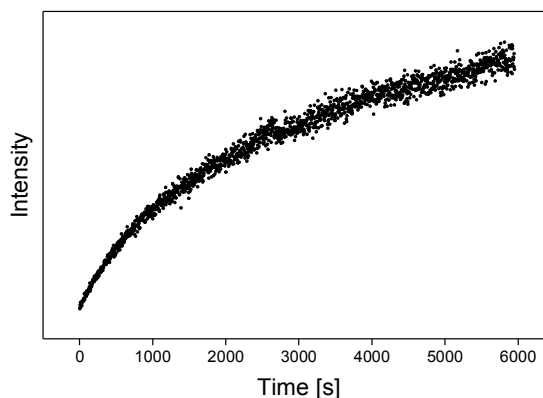


4 298 also has to be considered. This would be analogous to the formation of NC_6N from two C_3N^*
5 299 radicals, elucidated basing on the kinetics of HC_3N photolysis in rare gas matrices.²¹ Reaction 3 is
6 300 however not expected to be of chief importance here, considering the shape of the curve of growth
7 301 obtained for the $NC_{10}N$ phosphorescence during the photolysis of HC_5N in solid Kr (Figure 5). If the
8 302 photolysis of matrix-isolated HC_5N molecules had led to $NC_{10}N$ via the recombination of C_5N^*
9 303 radicals then, assuming the validity of arguments provided in Ref. ²¹ (reporting on the appearance of
10 304 NC_6N in irradiated HC_3N), one would have seen the original *increase* of the dinitrile production rate
11 305 with photolysis time. In the present case, the production rate steadily *decreases* from the very onset
12 306 of irradiations.

13
14
15
16 307 Creation of the discussed long, all-heavy-atom chain species requires substantial mobility of the
17 308 involved precursor chains, apart from their dehydrogenation. Locally increased mobility of reaction
18 309 partners may be understood in terms of matrix "melting" resultant from the dissipation of the
19 310 electronic excitation energy. Other products (including mono- and dicyanopolyynes) were detected
20 311 in the described experiments, but it was not possible to thoroughly investigate their formation
21 312 efficiencies in terms of kinetics and relative quantum yields.

22
23
24
25 313 It is also possible that the precursors, instead of being dissociated into free radicals, are excited to
26 314 high electronic energy levels and then undergo reactions analogous to Reaction 2. In experiments
27 315 described here, it is not possible to differentiate between the two cases.

28
29
30 316



44 317

44 318 **Figure 5. Time evolution of $NC_{10}N$ formation, as monitored by intensity of phosphorescence emitted from**
45 319 **irradiated (193 nm) Kr-isolated HC_5N . The abscissa represents the irradiation time.**

46
47 320

48 321 CONCLUSIONS

49
50 322 The synthesis of a dicyanopolyyne chain as long as $NC_{10}N$ via UV-induced coupling of smaller
51 323 molecules was observed in Ar and Kr matrices. Strong phosphorescence of $NC_{10}N$ was detected.
52 324 Vibronic patterns in phosphorescence and phosphorescence excitation spectra were partly
53 325 interpreted with the assistance of quantum chemical calculations. Among some general trends
54 326 observed in the series of cryogenic matrix-isolated $NC_{2n}N$ molecules is the lack of fluorescence,
55 327 which seems to be due to efficient intersystem crossing. Phosphorescence is dominated by a
56
57
58
59
60

1
2 328 vibronic progression involving a specific σ_g mode (an in-phase C≡C stretching). With increasing
3 329 length of the chain:

4
5 330 (i) the wavenumber of that particular mode decreases, approaching the limit defined by the pure
6 331 collective C≡C stretch of an infinite chain, with vanishing contributions from terminal C≡N groups;

7
8 332 (ii) phosphorescence origin bands become more and more prominent; their wavelengths closely
9 333 follow a Lewis-Calvin relation (linearity of $\lambda_{\text{origin}}^2$ vs. n);

10
11 334 (iii) energy of the first allowed ($^1\Sigma_u^+ - ^1\Sigma_g^+$) transition decreases.

12
13
14 335 Vibronic progressions observed for the $^1\Sigma_u^+ - ^1\Sigma_g^+$ system are governed by the same specific σ_g
15 336 stretching that shapes the phosphorescence spectrum. Its energy is lower in the excited state,
16 337 reflecting a decrease of the C≡C bond strength, compared to the ground state.

17
18
19 338 Phosphorescence measurement was a detection method of choice in this study aimed at molecule
20 339 coupling products. The quantity of synthesized $C_{10}N_2$ was too low to produce a detectable IR
21 340 signature. The reported experimental approach can presumably be adopted to synthesize and study
22 341 the $NC_{2n}N$ chains of $n > 5$; in particular, present results permit to expect the origin of $NC_{12}N$
23 342 phosphorescence in solid Kr at about 670 nm.

24
25
26 343

27 28 344 ACKNOWLEDGMENTS

29
30 345 This work was financially supported by the Polish National Science Centre, project no.
31 346 2011/03/B/ST4/02763, French-Polish scientific cooperation programs *Partenariat Hubert-Curien*
32 347 *Polonium* (2012-2013) and *PICS* (2014-2016). U.S. is a beneficiary of the French Government
33 348 scholarship *Bourse Eiffel*, managed by Campus France, and of the project “Scholarships for PhD
34 349 students of Podlaskie Voivodeship” – the project is co-financed by European Social Fund, Polish
35 350 Government and Podlaskie Voivodeship. J.-C.G. acknowledges the financial support received from
36 351 the Centre National d’Etudes Spatiales (CNES) and from the French program Physique et Chimie du
37 352 Milieu Interstellaire (PCMI) of CNRS/INSU with INC/INP co-funded by CEA and CNES.

38 39 353 SUPPORTING INFORMATION AVAILABLE

40
41 354 Geometry of $NC_{10}N$ in several electronic states; computed IR wavenumbers for the lowest excited
42 355 electronic states; visualization of vibrational modes in selected electronic states of $NC_{10}N$. This
43 356 information is available free of charge via the Internet at <http://pubs.acs.org>.

44
45 357

46 47 359 REFERENCES

- 48
49 360 (1) Schermann, G.; Grösser, T.; Hampel, F.; Hirsch, A. Dicyanopolyynes: A Homologous Series
50 361 of End-Capped Linear sp Carbon. *Chem. – Eur. J.* **1997**, *3*, 1105–1112.
51 362 (2) Turowski, M.; Crépin, C.; Couturier-Tamburelli, I.; Piétri, N.; Kołos, R. Low-Temperature
52 363 Phosphorescence of Dicyanoacetylene in Rare Gas Solids. *Low Temp. Phys.* **2012**, *38*, 723–
53 364 726.
54 365 (3) Trolez, Y.; Guillemin, J.-C. Synthesis and Characterization of 2,4-Pentadiynenitrile—A Key
55 366 Compound in Space Science. *Angew. Chem. Int. Ed.* **2005**, *44*, 7224–7226.
56 367 (4) Hunsmann, W. Nachweis Und Synthese Des Triacetylen. *Chem. Ber.* **1950**, *83*, 213–217.

- 1
2 368 (5) Ding, H.; Boguslavskiy, A. E.; Schmidt, T. W.; Maier, J. P. Gas Phase Electronic Spectrum of
3 369 the Nitrogen Terminated Nanowire NC₁₆N. *Chem. Phys. Lett.* **2004**, *392*, 225–228.
- 4 370 (6) Duley, W. W. Chemical Evolution of Carbonaceous Material in Interstellar Clouds.
5 371 *Astrophys. J.* **2000**, *528*, 841.
- 6 372 (7) Turner, B. E. Detection of Interstellar Cyanoacetylene. *Astrophys. J. Lett.* **1971**, *163*, L35.
- 7 373 (8) Dickinson, D. F. Detection of Cyanoacetylene at 18 GHz. *Astrophys. Lett.* **1972**, *12*, 235–236.
- 8 374 (9) McGee, R. X.; Balister, M.; Newton, L. M. Interstellar Cyanoacetylene J=2→1, J=4→3
9 375 Transitions. *Mon. Not. R. Astron. Soc.* **1977**, *180*, 585–592.
- 10 376 (10) Gardner, F. F.; Winnewisser, G. Observations of the J = 1→0 Transitions of the (13) C
11 377 Isotopic Species of Cyanoacetylene (HCCCN) in the Direction of Sagittarius B2. *Astrophys.*
12 378 *J.* **1975**, *197*, L73.
- 13 379 (11) Mauersberger, R.; Henkel, C.; Sage, L. J. Dense Gas in Nearby Galaxies. III - HC₃N as an
14 380 Extragalactic Density Probe. *Astron. Astrophys.* **1990**, *236*, 63–68.
- 15 381 (12) Bockelée-Morvan, D.; Lis, D. C.; Wink, J. E.; Despois, D.; Crovisier, J.; Bachiller, R.;
16 382 Benford, D. J.; Biver, N.; Colom, P.; Davies, J. K.; et al. New Molecules Found in Comet
17 383 C/1995 O1 (Hale-Bopp). Investigating the Link between Cometary and Interstellar Material.
18 384 *Astron. Astrophys.* **2000**, *353*, 1101–1114.
- 19 385 (13) Snell, R. L.; Schloerb, F. P.; Young, J. S.; Hjalmarsen, A.; Friberg, P. Observations of HC₃N,
20 386 HC₅N, and HC₇N in Molecular Clouds. *Astrophys. J.* **1981**, *244*, 45–53.
- 21 387 (14) Broten, N. W.; Oka, T.; Avery, L. W.; MacLeod, J. M.; Kroto, H. W. The Detection of HC₉N
22 388 in Interstellar Space. *Astrophys. J.* **1978**, *223*, L105.
- 23 389 (15) Truong-Bach; Graham, D.; Nguyen-Q-Rieu. HC₉N from the Envelopes of IRC+10216 and
24 390 CRL:2688. *Astron. Astrophys.* **1993**, *277*, 133.
- 25 391 (16) Bell, M. B.; Avery, L. W.; MacLeod, J. M.; Matthews, H. E. The Excitation Temperature of
26 392 HC₉N in the Circumstellar Envelope of IRC + 10216. *Astrophys. J.* **1992**, *400*, 551–555.
- 27 393 (17) Khanna, R. K.; Perera-Jarmer, M. A.; Ospina, M. J. Vibrational Infrared and Raman Spectra
28 394 of Dicyanoacetylene. *Spectrochim. Acta Part Mol. Spectrosc.* **1987**, *43*, 421–425.
- 29 395 (18) Agúndez, M.; Cernicharo, J.; Vicente, P. de; Marcelino, N.; Roueff, E.; Fuente, A.; Gerin, M.;
30 396 Guélin, M.; Albo, C.; Barcia, A.; et al. Probing Non-Polar Interstellar Molecules through
31 397 Their Protonated Form: Detection of Protonated Cyanogen (NCCNH⁺). *Astron. Astrophys.*
32 398 **2015**, *579*, L10.
- 33 399 (19) Waite, J. H.; Young, D. T.; Cravens, T. E.; Coates, A. J.; Crary, F. J.; Magee, B.; Westlake, J.
34 400 The Process of Tholin Formation in Titan's Upper Atmosphere. *Science* **2007**, *316*, 870–875.
- 35 401 (20) Woon, D. E.; Herbst, E. Quantum Chemical Predictions of the Properties of Known and
36 402 Postulated Neutral Interstellar Molecules. *Astrophys. J. Suppl. Ser.* **2009**, *185*, 273–288.
- 37 403 (21) Crépin, C.; Turowski, M.; Ceponkus, J.; Douin, S.; Boyé-Péronne, S.; Gronowski, M.; Kołos,
38 404 R. UV-Induced Growth of Cyanopolyynes Chains in Cryogenic Solids. *Phys. Chem. Chem.*
39 405 *Phys. PCCP* **2011**, *13*, 16780–16785.
- 40 406 (22) Turowski, M.; Crépin, C.; Douin, S.; Kołos, R. Formation and Spectroscopy of
41 407 Dicyanotriacetylene (NC₈N) in Solid Kr. *J. Phys. Chem. A* **2014**, *119*, 2701–2708.
- 42 408 (23) Chang, J.-W.; Lee, Y.-P. The C₂N₂ $\tilde{a}^3\Sigma_u^+ - \tilde{X}^1\Sigma_g^+$ Chemiluminescence in Matrices. *J. Mol.*
43 409 *Struct.* **1987**, *157*, 155–165.
- 44 410 (24) Smith, A. M.; Schallmoser, G.; Thoma, A.; Bondybey, V. E. Infrared Spectral Evidence of
45 411 N≡C–C≡C–N≡C: Photoisomerization of N≡C–C≡C–C≡N in an Argon Matrix. *J. Chem. Phys.*
46 412 **1993**, *98*, 1776–1785.
- 47 413 (25) Cataldo, F. Polyynes: A New Class of Carbon Allotropes. About the Formation of
48 414 Dicyanopolyynes from an Electric Arc between Graphite Electrodes in Liquid Nitrogen.
49 415 *Polyhedron* **2004**, *23*, 1889–1896.

- 1
2 416 (26) Cataldo, F. Polyynes and Cyanopolyynes: Their Synthesis with the Carbon Arc Gives the
3 417 Same Abundances Occurring in Carbon-Rich Stars. *Orig. Life Evol. Biospheres* **2006**, *36*,
4 418 467–475.
- 5 419 (27) Forte, G.; D’Urso, L.; Fazio, E.; Patanè, S.; Neri, F.; Puglisi, O.; Compagnini, G. The Effects
6 420 of Liquid Environments on the Optical Properties of Linear Carbon Chains Prepared by Laser
7 421 Ablation Generated Plasmas. *Appl. Surf. Sci.* **2013**, *272*, 76–81.
- 8 422 (28) Szczepaniak, U.; Kołos, R.; Gronowski, M.; Chevalier, M.; Guillemin, J.-C.; Turowski, M.;
9 423 Custer, T.; Crépin, C. Cryogenic Photochemical Synthesis and Electronic Spectroscopy of
10 424 Cyanotetracetylene. *J. Phys. Chem. A* **2017**, *121*, 7374–7384.
- 11 425 (29) Agreiter, J.; Smith, A. M.; Härtle, M.; Bondybey, V. E. Laser-Induced Fluorescence of
12 426 Matrix-Isolated $C_4N_2^+$. *Chem. Phys. Lett.* **1994**, *225*, 87–96.
- 13 427 (30) Agreiter, J.; Smith, A. M.; Bondybey, V. E. Laser-Induced Fluorescence of Matrix-Isolated
14 428 $C_6N_2^+$ and of $C_8N_2^+$. *Chem. Phys. Lett.* **1995**, *241*, 317–327.
- 15 429 (31) Coupeaud, A.; Kołos, R.; Couturier-Tamburelli, I.; Aycard, J. P.; Piétri, N. Photochemical
16 430 Synthesis of the Cyanodiacetylene HC_5N : A Cryogenic Matrix Experiment. *J. Phys. Chem. A*
17 431 **2006**, *110*, 2371–2377.
- 18 432 (32) Couturier-Tamburelli, I.; Piétri, N.; Crépin, C.; Turowski, M.; Guillemin, J.-C.; Kołos, R.
19 433 Synthesis and Spectroscopy of Cyanotriacetylene (HC_7N) in Solid Argon. *J. Chem. Phys.*
20 434 **2014**, *140*, 044329.
- 21 435 (33) Szczepaniak, U.; Kołos, R.; Gronowski, M.; Guillemin, J.-C.; Crépin, C. Low Temperature
22 436 Synthesis and Phosphorescence of Methylcyanotriacetylene. *J. Phys. Chem. A* **2018**, *122*, 89–
23 437 99.
- 24 438 (34) Parr, R. G.; Yang, W. *Density-Functional Theory of Atoms and Molecules*; Oxford University
25 439 Press, 1989.
- 26 440 (35) Frisch, M. J.; Trucks, G. W.; Schlegel, H. B.; Scuseria, G. E.; Robb, M. A.; Cheeseman, J. R.;
27 441 Scalmani, G.; Barone, V.; Mennucci, B.; Petersson, G. A.; et al. *Gaussian 09 Rev. B.01*;
28 442 Gaussian, Inc.: Wallingford, CT, USA, 2009.
- 29 443 (36) Bauernschmitt, R.; Ahlrichs, R. Treatment of Electronic Excitations within the Adiabatic
30 444 Approximation of Time Dependent Density Functional Theory. *Chem. Phys. Lett.* **1996**, *256*,
31 445 454–464.
- 32 446 (37) Casida, M. E.; Jamorski, C.; Casida, K. C.; Salahub, D. R. Molecular Excitation Energies to
33 447 High-Lying Bound States from Time-Dependent Density-Functional Response Theory:
34 448 Characterization and Correction of the Time-Dependent Local Density Approximation
35 449 Ionization Threshold. *J. Chem. Phys.* **1998**, *108*, 4439–4449.
- 36 450 (38) Stratmann, R. E.; Scuseria, G. E.; Frisch, M. J. An Efficient Implementation of Time-
37 451 Dependent Density-Functional Theory for the Calculation of Excitation Energies of Large
38 452 Molecules. *J. Chem. Phys.* **1998**, *109*, 8218–8224.
- 39 453 (39) Perdew, J. P.; Ziesche, P.; Eschrig, H. *Electronic Structure of Solids’ 91*; Akademie Verlag,
40 454 Berlin, 1991; Vol. 11.
- 41 455 (40) Perdew, J. P.; Chevary, J. A.; Vosko, S. H.; Jackson, K. A.; Pederson, M. R.; Singh, D. J.;
42 456 Fiolhais, C. Atoms, Molecules, Solids, and Surfaces: Applications of the Generalized
43 457 Gradient Approximation for Exchange and Correlation. *Phys. Rev. B* **1992**, *46*, 6671–6687.
- 44 458 (41) Perdew, J. P.; Chevary, J. A.; Vosko, S. H.; Jackson, K. A.; Pederson, M. R.; Singh, D. J.;
45 459 Fiolhais, C. Erratum: Atoms, Molecules, Solids, and Surfaces: Applications of the
46 460 Generalized Gradient Approximation for Exchange and Correlation. *Phys. Rev. B* **1993**, *48*,
47 461 4978–4978.
- 48 462 (42) Perdew, J. P.; Burke, K.; Wang, Y. Generalized Gradient Approximation for the Exchange-
49 463 Correlation Hole of a Many-Electron System. *Phys. Rev. B* **1996**, *54*, 16533–16539.

- 1
2 464 (43) Yanai, T.; Tew, D. P.; Handy, N. C. A New Hybrid Exchange–correlation Functional Using
3 465 the Coulomb-Attenuating Method (CAM-B3LYP). *Chem. Phys. Lett.* **2004**, *393*, 51–57.
- 4 466 (44) Dunning, T. H. J. Gaussian Basis Sets for Use in Correlated Molecular Calculations. I. The
5 467 Atoms Boron through Neon and Hydrogen. *J. Chem. Phys.* **1989**, *90*, 1007–1023.
- 6 468 (45) Kendall, R. A.; Jr, T. H. D.; Harrison, R. J. Electron Affinities of the First-Row Atoms
7 469 Revisited. Systematic Basis Sets and Wave Functions. *J. Chem. Phys.* **1992**, *96*, 6796–6806.
- 8 470 (46) Andersson, M. P.; Uvdal, P. New Scale Factors for Harmonic Vibrational Frequencies Using
9 471 the B3LYP Density Functional Method with the Triple- ζ Basis Set 6-311+G(d,P). *J. Phys.*
10 472 *Chem. A* **2005**, *109*, 2937–2941.
- 11 473 (47) Merrick, J. P.; Moran, D.; Radom, L. An Evaluation of Harmonic Vibrational Frequency
12 474 Scale Factors. *J. Phys. Chem. A* **2007**, *111*, 11683–11700.
- 13 475 (48) Foresman, J. B.; Head-Gordon, M.; Pople, J. A.; Frisch, M. J. Toward a Systematic Molecular
14 476 Orbital Theory for Excited States. *J. Phys. Chem.* **1992**, *96*, 135–149.
- 15 477 (49) Christiansen, O.; Koch, H.; Jørgensen, P. The Second-Order Approximate Coupled Cluster
16 478 Singles and Doubles Model CC2. *Chem. Phys. Lett.* **1995**, *243*, 409–418.
- 17 479 (50) Christiansen, O.; Koch, H.; Halkier, A.; Jørgensen, P.; Helgaker, T.; Merás, A. S. de. Large-
18 480 scale Calculations of Excitation Energies in Coupled Cluster Theory: The Singlet Excited
19 481 States of Benzene. *J. Chem. Phys.* **1996**, *105*, 6921–6939.
- 20 482 (51) Christiansen, O.; Halkier, A.; Koch, H.; Jørgensen, P.; Helgaker, T. Integral-Direct Coupled
21 483 Cluster Calculations of Frequency-Dependent Polarizabilities, Transition Probabilities and
22 484 Excited-State Properties. *J. Chem. Phys.* **1998**, *108*, 2801–2816.
- 23 485 (52) Hald, K.; Hättig, C.; Jørgensen, P. Triplet Excitation Energies in the Coupled Cluster Singles
24 486 and Doubles Model Using an Explicit Triplet Spin Coupled Excitation Space. *J. Chem. Phys.*
25 487 **2000**, *113*, 7765–7772.
- 26 488 (53) Aidas, K.; Angeli, C.; Bak, K. L.; Bakken, V.; Bast, R.; Boman, L.; Christiansen, O.;
27 489 Cimiraaglia, R.; Coriani, S.; Dahle, P.; et al. The Dalton Quantum Chemistry Program System.
28 490 *Wiley Interdiscip. Rev. Comput. Mol. Sci.* **2014**, *4*, 269–284.
- 29 491 (54) Angeli, C.; Bak, K. L.; Bakken, V.; Christiansen, O.; Cimiraaglia, R.; Coriani, S.; Dahle, P.;
30 492 Dalskov, E. K.; Enevoldsen, T.; Fernandez, B.; et al. *Dalton, a Molecular Electronic*
31 493 *Structure Program, Release Dalton2016.2* (2016), see <http://Daltonprogram.org>.
- 32 494 (55) Zhurko, G. *Chemcraft - Graphical program for visualization of quantum chemistry*
33 495 *computations* <http://chemcraftprog.com/>.
- 34 496 (56) Turowski, M.; Szczepaniak, U.; Custer, T.; Gronowski, M.; Kołos, R. Electronic
35 497 Spectroscopy of Methylcyanodiacetylene ($\text{CH}_3\text{C}_5\text{N}$). *ChemPhysChem* **2016**, *17*, 4068–4078.
- 36 498 (57) Turowski, M. Niskotemperaturowe Badania Fotochemii i Spektroskopii Cyjanoacetylenów o
37 499 Znaczeniu Astrofizycznym. PhD Dissertation, Institute of Physical Chemistry, Polish
38 500 Academy of Sciences, Warsaw, 2012.
- 39 501 (58) Turowski, M.; Crépin, C.; Gronowski, M.; Guillemin, J.-C.; Coupeaud, A.; Couturier-
40 502 Tamburelli, I.; Piétri, N.; Kołos, R. Electronic Absorption and Phosphorescence of
41 503 Cyanodiacetylene. *J. Chem. Phys.* **2010**, *133*, 074310–074310.
- 42 504 (59) Murrell, J. N. *The Theory of the Electronic Spectra of Organic Molecules*; Methuen & Co.
43 505 Ltd: London, U.K., 1963.
- 44 506 (60) Kuhn, H. A Quantum-Mechanical Theory of Light Absorption of Organic Dyes and Similar
45 507 Compounds. *J. Chem. Phys.* **1949**, *17*, 1198–1212.
- 46 508 (61) Lewis, G. N.; Calvin, M. The Color of Organic Substances. *Chem. Rev.* **1939**, *25*, 273–328.
- 47 509 (62) Forney, D.; Freivogel, P.; Fulara, J.; Maier, J. P. Electronic Absorption Spectra of Cyano-
48 510 substituted Polyacetylene Cations in Neon Matrices. *J. Chem. Phys.* **1995**, *102*, 1510–1514.
- 49 511 (63) Pino, T.; Ding, H.; Güthe, F.; Maier, J. P. Electronic Spectra of the Chains HC_{2n}H ($n=8-13$)
50 512 in the Gas Phase. *J. Chem. Phys.* **2001**, *114*, 2208–2212.

- 1
2 513 (64) Hausser, K. W.; Kuhn, R.; Seitz, G. Lichtabsorption Und Doppelbindung. V. Über Die
3 514 Absorption von Verbindungen Min Konjugierten Kohlenstoffdoppelbindungen Bei Tiefer
4 515 Temperatur. *Z Phys. Chem Abt B* **1935**, *29*, 391.
5 516 (65) Connors, R. E.; Roebber, J. L.; Weiss, K. Vacuum Ultraviolet Spectroscopy of Cyanogen and
6 517 Cyanoacetylenes. *J. Chem. Phys.* **1974**, *60*, 5011–5024.
7 518
8 519
9

10

11

12

13

14

15

16

17

18

19

20

21

22

23

24

25

26

27

28

29

30

31

32

33

34

35

36

37

38

39

40

41

42

43

44

45

46

47

48

49

50

51

52

53

54

55

56

57

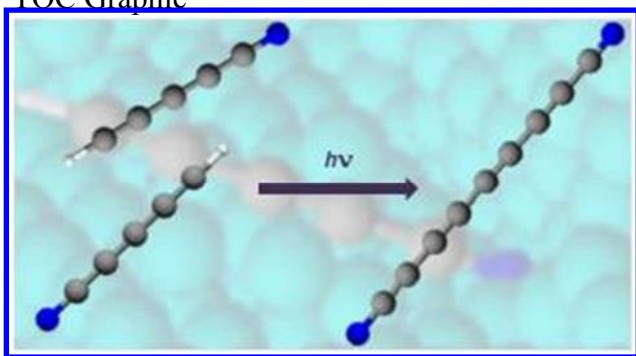
58

59

60

1
2
3
4
5
6
7
8
9
10
11
12
13
14
15
16
17
18
19
20
21
22
23
24
25
26
27
28
29
30
31
32
33
34
35
36
37
38
39
40
41
42
43
44
45
46
47
48
49
50
51
52
53
54
55
56
57
58
59
60
520

TOC Graphic

521
522